UNIVERSIDAD NACIONAL AUTÓNOMA DE MÉXICO

FACULTAD DE INGENIERÍA

Coastline variability of several Latin American cities alongside Pacific Ocean due to the unusual "Sea Swell" events of 2015

ARTÍCULO ACADÉMICO

Que para obtener el título de

Ingeniero Geofísico

P R E S E N T A

Francisco Reyes Hernández

ASESOR DE ARTÍCULO ACADÉMICO

M. ED. Miguel Ildefonso Vera Ocampo

Ciudad Universitaria, Cd. Mx., 2021

Environ Monit Assess (2020) 192:522
https://doi.org/10.1007/s10661-020-08469-x

Coastline variability of several Latin American cities alongside Pacific Ocean due to the unusual "Sea Swell" events of 2015

P. Godwyn-Paulson · M. P. Jonathan · Francisco Reyes Hernandez · G. Muthusankar · C. Lakshumanan

Received: 6 February 2020 / Accepted: 29 June 2020

Abstract This study aims to report the short-term coastline dynamics and inundation limits of coastal cities along the Eastern Pacific due to the sea swell events that occurred during April to May 2015. The multi-temporal satellite datasets from Landsat such as Enhanced Thematic Mapper (L7 ETM+) and Operational Land Imager/Thermal Infrared Sensor (L8 OLI/TIRS) of different periods before and after the swell events were used to identify the shoreline changes. The satellite images were pre-processed using ERDAS imagine 9.2, and the coastline was digitized in ArcGIS 10.4.1 for ten cities spread across from Mexico to Chile (in Pacific coast) using the spectral water indices, and the shoreline change rate and erosion/accretion pattern at each transect were estimated using the statistical parameters embedded in Digital Shoreline Analysis System (DSAS). The maximum erosion and accretion were observed in El Salvador (268 m) and Huatulco (Mexico) (115 m), respectively. Likewise, the maximum inundation was observed in El Salvador with 268 m and Acapulco (Mexico) with 254 m, and the tide gauge data suggest a possible relation to the bathymetry and the geomorphological conditions of the coast. Overall, the results indicate that the Eastern Pacific Ocean side sea swell events has led to extreme coastal flooding in recent years due to the increase in the mean sea level and the unpredictable variation in El Niño/Southern Oscillation events.

Keywords Sea swell 2015 · Coastal cities · Inundation · El Niño/Southern Oscillation · DSAS · Latin American countries

Abbreviations

ACE	Accumulated Cyclone Energy
CENAPRED	Centro Nacional de Prevención de Desastres (National Center for Disaster Prevention)
CONAGUA	Comisión Nacional del Agua, Mexico (National Water Commission)
DSAS	Digital Shoreline Analysis System
ENSO	El Niño Southern Oscillation
ESRI	Environmental System Research Institute
GLS	Geographical Information System
L7ETM	Landsat Enhanced Thematic Mapper
LAC	Latin American countries

Electronic supplementary material The online version of this article (https://doi.org/10.1007/s10661-020-08469-x) contains supplementary material, which is available to authorized users.

P. Godwyn-Paulson · M. P. Jonathan (✉) · F. R. Hernandez
Centro Interdisciplinario de Investigaciones y Estudios sobre Medio Ambiente y Desarrollo (CIIEMAD), Instituto Politécnico Nacional (IPN), Calle 30 de Junio de 1520, Barrio la Laguna Ticomán, Del. Gustavo A. Madero, C.P.07340, Ciudad de Mexico (CDMX), Mexico
e-mail: mpjonathan7@yahoo.com

G. Muthusankar
French Institute of Pondicherry, 11 St Louis Street, P.B. 33, Puducherry 605001, India

C. Lakshumanan
Centre for Remote Sensing, Bharathidasan University, Khajamalai Campus, Tiruchirappalli 620023, India

Published online: 15 July 2020

MNDWI	Modified Normalized Difference Water Index
Mts	Meters
NSM	Net Shoreline Movement
ONEMI	Oficina Nacional de Emergencia del Ministerio del Interior y Seguridad Publica, Chile (National Emergency Office of the Ministry of Interior)
SCE	Shoreline Change Envelope
SLR	Sea level rise
SMN	Servicio Meteorológico Nacional, Mexico (National Meteorological Service)
SSE	Sea swell events
TPMC	Technology Planning and Management Corporation
USGS	United State Geological Survey

Introduction

Coastal zone is a dynamic interface between land and sea with intense human activities (Yu et al. 2019). The coastal communities are frequently affected by natural calamities like tropical storms and hurricanes, which bring strong winds, huge waves, extreme rainfalls, and storm surges (Scott and Ramsay 2014). Storm surge, a rise in sea surface level due to atmospheric forcing, wind drag, and pressure (Muis et al. 2016), is the main cause of coastal flooding and erosion (Wong et al. 2014). However, it has been recognized that long-wavelength wind waves known as "Swells" produced by distant storms can propagate faster across an entire ocean basin by gaining momentum and energy across the ocean (Jiang and Chen 2013). Similar to tsunami waves, swell waves can also cause potential risk to coastal communities, damage to infrastructure, and beach erosion due to their low dissipation rate and long distant propagation (de Farias et al. 2012). Swell dispersion additionally generates infra-gravity waves causing an uprush in the wave run-up while reaching the shore creating unpredictable damage to coastal zone (Hoeke et al. 2013). The concurrence of waves with spring high tides and long fetching strong winds are often devastating in the highly populated coastal cities (Lyddon et al. 2019). Moreover, studies by Palmer et al. (2019) on the rise of global mean rate of sea level rise (SLR) indicate that it is increasing at a rate of 0.084 ± 0.025 mm yr^{-2} and the coastal flooding in different regions is mainly due to the SLR that affects often the nearly 10% of the Earth's population living along the coast (Wdowinski et al. 2016). Recent research has confirmed that the Eastern tropical and North Eastern Pacific sea level is increasing due to ENSO (El Niño Southern Oscillation) and Pacific Decadal Oscillation for the past two decades (Hamlington et al. 2016). Hence, the severity and duration of flooding will increase in low-lying coastal communities as a result of the changes in wave dynamics (Vitousek et al. 2017).

The extreme wave events in the coastal region are usually measured through tide gauge station, while field survey is done to identify the high-water marks through GPS technique. Tide gauges in the coasts provide accurate information on different high-energy wave-related events where it shows the sea level rise on a regional and global scale. Tide gauges, however, are limited to a single point and cannot acquire information through a continuous spatial extent of a storm-induced swells, whereas the post-surge field survey is expensive and laborious to generate the complete dataset (Brakenridge et al. 2013). Recently, detecting and monitoring the flood events globally are made easier using geospatial techniques encompassing the bird's-eye perspective with high-resolution multispectral data. The satellite imagery obtained from Landsat data offers repeatable imagery for every 16 days to present. The US Geological Survey (USGS) in 2008 released the entire dataset of Landsat archive to the public to develop the studies related to land/water dynamics (Olthof et al. 2015). Landsat satellite images are being extensively used for surface water mapping by classifying pixels as either water or land through hard classification methods (Foody 2000; Halabisky et al. 2016).

Eastern Pacific Ocean information

The Pacific coast of Latin America includes the continental countries of Americas from Mexico in the Central American region to Chile in the south. The population in low elevation coastal zone is increasing globally, and it is estimated to increase by 230% by 2030 (Rojas et al. 2017). It is estimated that 29 to 32 million people are living within 10-m elevation of sea level in the Latin America and Caribbean coasts as per records during the start of the century (Reguero et al. 2015). The economy of Latin American countries (LAC) is mainly dependent on tourism and natural resources which is also exposed to long-term damages due to ENSO-related climate

change events (Delgado-Serrano et al. 2017). The Eastern Pacific region is one of the most prolific storm-forming regions in the world with an average of 16.5/year named storms during the period of 1981–2010, where 8.9 of those becoming hurricanes and 4.3 becoming major hurricanes. Thus, the Accumulated Cyclone Energy (ACE) index for the East Pacific basin during 2015 was 158 ($\times 10^4$ knots^2), which is above the 1981–2010 average of 132 ($\times 10^4$ knots^2) and the highest since 2006 (NOAA 2019). The Eastern Pacific being one of the most active basins with highest number of storms drives the importance of coastal inundation mapping in order to assess the damage incurred and to improve coastal management practices.

Moreover, the eastern coast of the Pacific experiences a seasonal (May–June) extreme wave events, which usually generates near the Antarctic ocean (50–60°S); this phenomenon is locally known as "*Mar de fondo*" and has become sensational throughout the country as a result of the damages caused by coastal flooding (Xavier et al. 2019).

The present study is focused on mapping the coastal inundation limit of several low-lying coastal cities along the eastern coast of Pacific from Mexico to Chile before and after the sea swell events (SSE), which occurred during April to May 2015 using remote sensing and Geographical Information System (GIS) tools.

Materials and methods

Description of the SSE

The massive swell events took place during the end of April (1st event: April 28–May 7) and in May (2nd event: 8 to 15; 3rd event: 18 to 27) 2015. This unusual phenomenon was triggered by the low-pressure system that originated from the South Pacific that usually produces extra tropical storms. Continuous and elevated waves travel more than 10,000 km due to strong wind action before making considerable damages along the coasts of Latin America (National Center for Disaster Prevention, CENAPRED). In Mexico, the National Meteorological Service (SMN) often warned all the coastal states from Chiapas to Jalisco for extreme waves of three to four meters height with heavy rain. The Maritime Meteorological Analysis and Forecasting Center of the Secretary of the Navy and the agency of the National Water Commission (CONAGUA) expected the waves to reach 1.5 to 2.5 m height on the coasts of Chiapas and Oaxaca. In Chile, the regional directorates of the National Emergency Office of the Ministry of the Interior (ONEMI) had issued an early warning for the coastal cities from Tarapaca to Aysen due to strong wind in the high seas, with large swells and very poor sea condition. In addition, civil protections in other Eastern Pacific countries also issued an emergency alert for the entire coastline.

Countries, namely, Chile, Peru, Ecuador, Colombia, Panama, Honduras, El Salvador, Guatemala, and Mexico all along the Pacific side were affected by the swell events among which El Salvador was the hardest hit. Ten coastal cities, namely, (1) Mazatlan (Mz), (2) Lazaro Cardenas (Lc), (3) Acapulco (Ac), (4) Puerto Angel (Pa), (5) Huatulco (Ht), (6) Salina Cruz (Sz) in Mexico, (7) Acajutla and La Libertad (El) in El Salvador, (8) Matarani (Mt) in Peru, (9) Arica (Ar), and (10) Antofagasta (Af) in Chile were selected based on damages and availability of data for the present study (Fig. 1) to compute the inundation limit/change in coastline before and after the swell events with the help of GIS tools.

Remote sensing data sources

Multi-temporal satellite images of Landsat 8 (Operational Land Imager, OLI/Thermal Infrared Sensor, TIRS) of different periods before and after the swell events were downloaded in GeoTIFF format through the US Geological Survey (USGS) Earth Explorer Website (https://www.earthexplorer.usgs.gov/). The cloud cover in all the images was selected to be less than 20% before downloading. The details of satellite data used for the study are shown in Table 1.

Image pre-processing

The raw satellite images cannot be used as a base map for analyzing shoreline changes without doing radiometric and geometric corrections (Sheik and Chandrasekar 2011). The acquired Landsat images were selected without stripping defect, and the radiometric correction was carried out for each band to reduce the atmospheric effect. Geo-reference processing was carried out using UTM coordinate system with WGS84 datum using ERDAS IMAGINE 9.2 software. Likewise, the Visible Green and Short-Wave Infrared (SWIR 1) bands were stacked separately for each location and were used for the study.

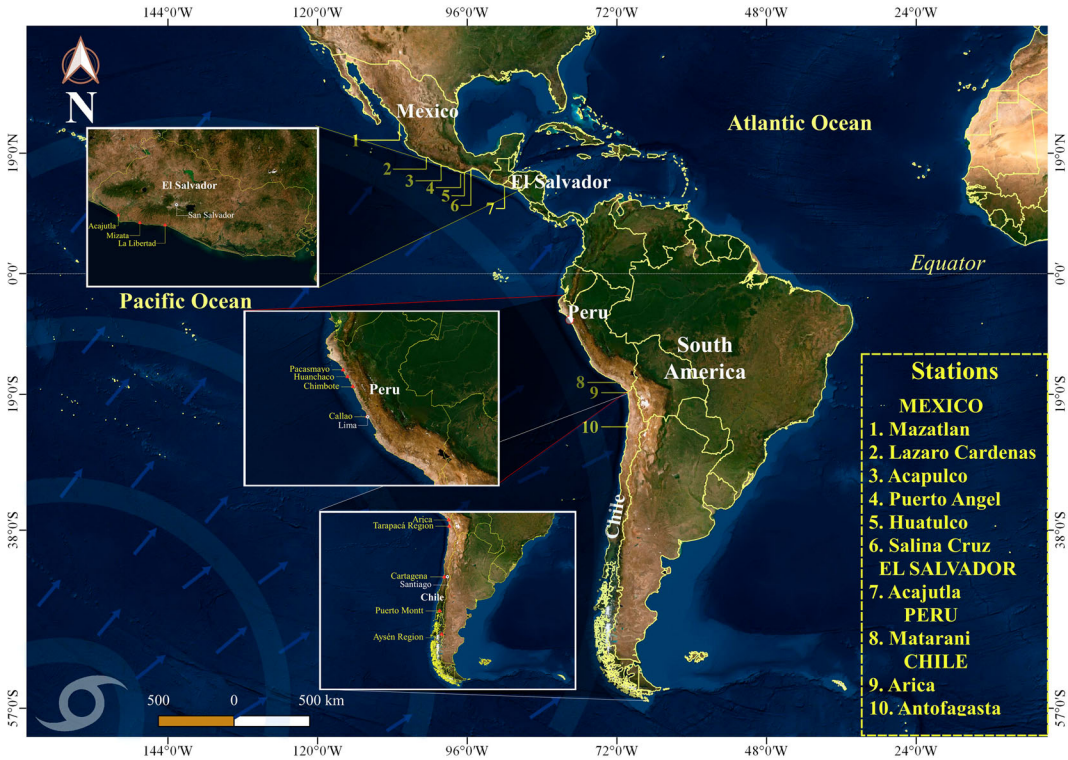

Fig. 1 Study area locations in North America [1–6: Mexico (1: Mazatlan; 2: Lazaro Cardenas; 3: Acapulco; 4: Puerto Angel; 5: Huatulco; 6: Salina Cruz)]; Central America [El Salvador (7: Acajutla)]; South America[Peru (8: Matarani); Chile (9: Arica; 10: Antofagasta)]

Extraction of inundation line

Remote sensing-based shoreline and water body extraction have become widespread approach including band rationing and water indices (Jeihouni et al. 2019). The water pixels and non-water pixels in a satellite image are generally differentiated using spectral water indices to identify the shoreline boundary. The Modified Normalized Difference Water Index (MNDWI) has improved the insight of pixels representing water bodies (Kelly and Gontz 2018) and has an outstanding advantage in executing coastline extraction (Wang et al. 2018). To extract the water information from satellite image, the digital number value of one spectral band is divided by the pixel value of another band to get the output raster and is expressed as follows:

$$\mathrm{MNDWI} = (\mathrm{Band}_3 - \mathrm{Band}_6)/(\mathrm{Band}_3 + \mathrm{Band}_6).$$

where Band_3 is the visible green band (0.53–0.59 μm) and Band_6 is the short-wave infrared band (1.57–1.65 μm).

Subsequently, after applying the water indices in ArcGIS 10.4.1, the output raster was subjected to classification and computed with the colors from green to blue to identify the land-water boundary. The pixels representing the built-up land, soil, and vegetation will have negative values closer to − 1, and the pixels representing water bodies will have positive values closer to + 1. Since the wet land area appears in blue color after classification, the inundation line of swell waves was extracted using ArcGIS.

Coastline change analysis

The Digital Shoreline Analysis System (DSAS), an open source extension of Environmental System Research Institute (ESRI)'s ArcGIS software developed jointly by USGS and TPMC environmental services is used in this study for the analysis of shoreline variations. The DSAS contains a proper user guide which allows the user to find the shoreline change analysis by defining a reference baseline for measurements and defining shorelines for calculating the rate of change statistics and automated or manual generation of measurement transect, which calculates the shoreline uncertainties using the inbuilt statistical methods. Two shorelines

Table 1 Specifications of the used satellite dataset

Acquisition date	Satellite/sensor	Path/row	Location	Zone
Mar 26, 2015	Landsat_8 / (OLI/TIRS)	31/44	Mazatlan	13
May 29, 2015	Landsat_8 / (OLI/TIRS)	31/44	Mazatlan	13
Apr 6, 2015	Landsat_8 / (OLI/TIRS)	28/48	Lazaro Cardenas	13
May 24, 2015	Landsat_8 / (OLI/TIRS)	28/48	Lazaro Cardenas	13
Mar 7, 2015	Landsat_8 / (OLI/TIRS)	26/48	Acapulco	14
May 26, 2015	Landsat_8 / (OLI/TIRS)	26/48	Acapulco	14
Mar 25, 2015	Landsat_8 / (OLI/TIRS)	24/49	Puerto Angel	14
May 28, 2015	Landsat_8 / (OLI/TIRS)	24/49	Puerto Angel	14
Apr 10, 2015	Landsat_8 / (OLI/TIRS)	24/49	Huatulco	14
May 28, 2015	Landsat_8 / (OLI/TIRS)	24/49	Huatulco	14
Apr 3, 2015	Landsat_8 / (OLI/TIRS)	23/49	Salina Cruz	15
May 21, 2015	Landsat_8 / (OLI/TIRS)	23/49	Salina Cruz	15
Feb 26, 2015	Landsat_7 / (ETM+)	19/51	El Salvador	16
Jun 2, 2015	Landsat_7 / (ETM+)	19/51	El Salvador	16
Mar 29, 2015	Landsat_8 / (OLI/TIRS)	4/72	Matarani	18
May 16, 2015	Landsat_8 / (OLI/TIRS)	4/72	Matarani	18
Mar 31, 2015	Landsat_8 / (OLI/TIRS)	2/73	Arica	19
May 18, 2015	Landsat_8 / (OLI/TIRS)	2/73	Arica	19
Mar 31, 2015	Landsat_8 / (OLI/TIRS)	2/76	Antofagasta	19
Jun 3, 2015	Landsat_8 / (OLI/TIRS)	2/76	Antofagasta	19

Spatial resolution: 30 m; coordinate system/datum: UTM/WGS84; data source: USGS

for each study location were drawn by identifying the water body using water indices (MNDWI), where the baseline was set up parallel to the shoreline with the distance of 20 m from the shoreline. The DSAS produces transect lines perpendicular to the baseline and across the two shorelines, and the transect lines were generated with 50-m interval. The intersections of transect shoreline along the baseline are used to calculate the shoreline variations before and after the swell events.

The shoreline movements were calculated in DSAS with the help of statistical values, while the landward movement of shoreline (i.e., erosion) will give negative values and the seaward movement of shoreline (i.e., accretion) will give positive values. Likewise, the erosion/accretion values will be calculated regardless of baseline orientation (Himmelstoss et al. 2018). DSAS contains several analytical processes, among which Net Shoreline Movement (NSM) and Shoreline Change Envelope (SCE) were used to calculate the short-term changes in shoreline with distance in meters. The NSM calculates the difference in distance between the oldest (before swell events) and the latest shoreline (after swell events). The above difference relates to the date, and only two shorelines are required to calculate the difference in each transects, and the results will be in negative and positive values. The SCE reports the maximum distance between any two shorelines, and the results will be in positive values only. Henceforth, for the present study, two DSAS methods were used to map the areas subjected to erosion and accretion after the swell events.

Tide gauge data

Tide gauges are installed to measure the water level at a specific location relative to the surface to which they are mounted and are the easily accessible source to attain the coastal sea level changes data (Becker et al. 2019). The sea level data for the tide gauge stations (a–f, Mexico; g, El Salvador; h, Peru; i–j, Chile in Fig. 2), namely, (a) Mazatlan, (b) Lazaro Cardenas, (c) Acapulco, (d) Puerto Angel, (e) Huatulco, (f) Salina Cruz, (g) Acajutla, (h) Matarani, (i) Arica, and (j) Antofagasta for the month of April 26 to May 31 (2015), were

downloaded from the sea level monitoring facility of the intergovernmental oceanographic commission of the UNESCO (http://www.ioc-sealevelmonitoring.org) website (Fig. 2). The tide gauge record was used to identify the maximum wave height during the swell events from April to May 2015 with a sampling interval of 1 min.

Results

Assessment of shoreline changes

The NSM-calculated values with the help of DSAS are presented in Figs. 3 and 4 (1–10), highlighting the NSM values for all the study locations in both negative and positive values, signifying the movement of shoreline landward (erosion) and seaward (accretion), respectively.

The landward movement was highly observed in El Salvador with the maximum value of – 268 mts at the transect number 760 followed by Acapulco in Mexico with the maximum value of – 254 mts at the transect number 587. Likewise, the maximum seaward movement was recorded in Huatulco (Mexico) with + 115 mts at the transect number 335. Acajutla and La Libertad are the largest ports in El Salvador where a majority of the coastal residents are concentrated very close to the shore. Acajutla has very low relief on its western side with lagoons and marshes, and the eastern side is steeper, which causes larger flooding area in the former and smaller flooding area in the latter region. La Libertad (in El Salvador) has steeper coast on its west and low-lying flat land on its east which is developed as a tourist region. All the above factors along with its proximity to the coast have increased the inundation limit in this region (Álvarez-Gómez et al. 2013). Likewise, Acapulco is characterized by the formation of low deltaic plains which has a major port and is known to have innumerous resorts and largest beach city with increased urbanization. Especially, surrounding Acapulco bay, the maximum inundation has been recorded due to the modification of natural vegetation into settlement area in between 1970 and 2010, where nearly 110 km^2 of vegetation land were transformed to urban civilization (Zuniga and Magaña 2018) (Video 1).

The tide gauge data for coastal cities of Mexico and Chile are represented in Fig. 2 a–j, which clearly indicates the occurrence of three distinct events, the first one during the end of April around 28 and the second and third event were recorded during May 8 to 15 and May 18 to 27, 2015, respectively. The tidal data also serves as an evidence for storm surge event hitting the Pacific coast during April–May 2015. The calculated residual tide variation observed in the coastal areas of Mexico during the three events varied from 0 to 1.27 mts, and it is mainly due to the local bathymetry variation in the offshore section, which often reflects the minimum and maximum height of inundation in these regions.

Table 2 shows the percentage of area subjected to landward movement with no change, whereas the seaward movement was detected in many places. The observed sites with highest percentage of landward motion is presented in the decreasing order of Af (84.1) > Lc (84.0) > Ht (80.3) > Mt (76.1) > Ac (73.0) > El (72.3) > Pa (57.4) > Sz (44.3) > Mz (33.2). Similarly, the percentage of area which underwent maximum seaward motion is grouped in decreasing order Mz (63.1) > Sz (33.1) > Ac (18.3) > Ht (16.7) > El (11.0) > Mt (8.0) ≥ Lc (8.0) > Pa (6.6) > Af (3.6), and the area which did not undergo any significant changes are Pa (35.8) > Sz (22.6) > El (16.7) > Mt (15.9) > Af (12.3) > Ac (8.7) > Lc (8.0) > Mz (3.7) > Ht (3.0). However, Arica (Ar) presented the highest value of 99.4% erosion because the satellite image used for the analysis was acquired during the occurrence of sea swell events, i.e., 18 May 2015.

The consideration of SCE, NSM, and wave height characteristics for the present study has been able to explore the temporal and spatial dynamics of sea swell episodes. The above process is due to their significance in estimating the largest distance between all shorelines (SCE), cumulative shoreline movement (NSM), and swell energies at specific time intervals (Sweet et al. 2015; Dereli and Tercan 2020). Shoreline change statistics for the present study represent a significant negative correlation ($r^2 = -0.95$, when $p < 0.05$) between NSM and SCE clearly demonstrating the high erosive rates generated by the sea swell events of 2015 (e.g., Martin et al. 2020).

Table 2 represents the movement in coastline position before and after the SSE events along different study locations in meters and are presented in decreasing order as follows: El (267.6) > Ac (253.5) > Lc (124.9) > Ht (114.5) > Af (103.2) > Mt (92.5) > Mz (62.2) > Pa (46.6) > Sz (33.0). The shorelines which are most vulnerable to coastal inundation presented in a decreasing order

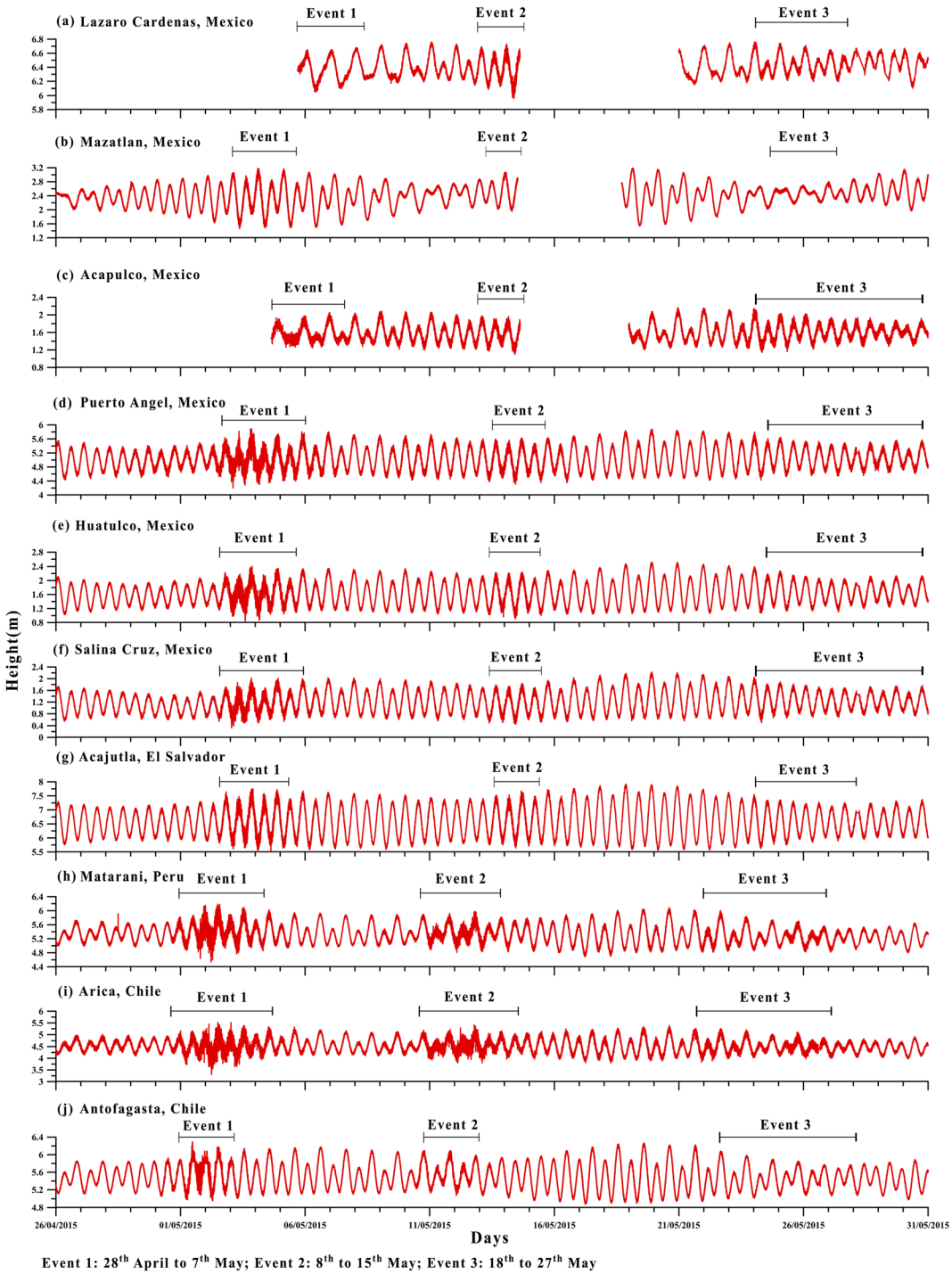

Fig. 2 **a**–**j** Graphs representing the tide gauge data from Chile and Mexican regions

on the basis of maximum inundation in meters are as follows: El (267.6) > Ac (253.5) > Lc (124.9) > Af (103.2) > Mt (92.5) > Ht (91.8) > Mz (53.9) > Pa (46.6) > Sz (33.0). However, El Salvador recorded the maximum wave height (2.35 mts) during the swell event, and the lowest was recorded in Lazaro Cardenas (0.54 mts).

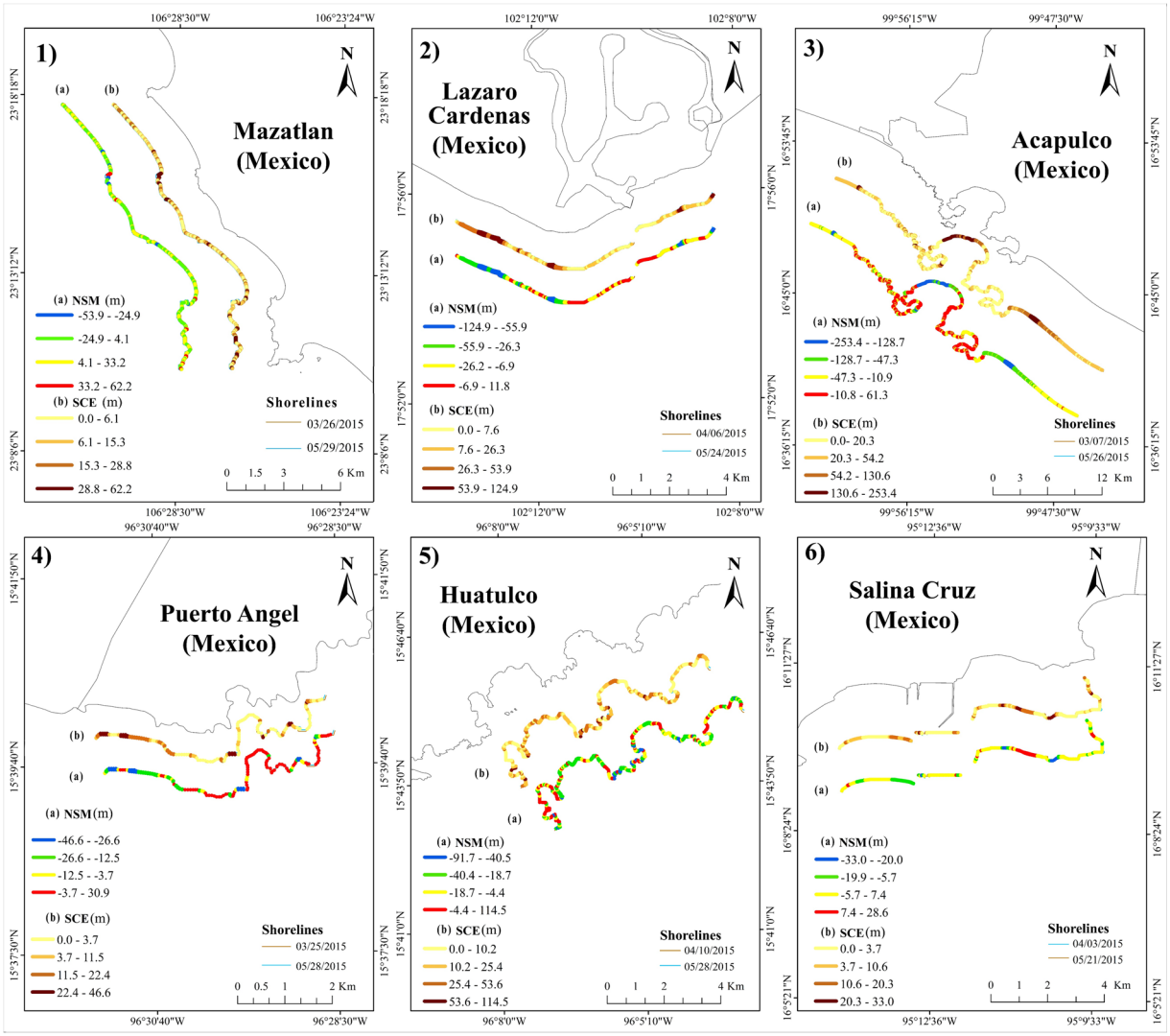

Fig. 3 (1–6) Shoreline change rates in the coasts of different study locations in Mexico, showing (a) Net Shoreline Movement (NSM) and (b) Shoreline Change Envelope (SCE)

Discussion

Factors responsible for SSE

The increase in sea level along the Pacific coastline of North and South America is documented to be the significant driving forces of sedimentary shoreline movements (Páez-Osuna et al. 2016). A couple of paired cyclones were generated during the early 2015 in the Western Pacific, which produced a strong westerly anomaly along the equator, whereas during the month of March to May (2015), the westerly wind events burst firmly which pushed the warm pool towards east and in turn the sea surface temperature anomaly in the Eastern Equatorial Pacific has increased as high as 4 °C (Hu and Fedorov 2016), leading to the super El Niño event of 2015. The warm ocean waters along the western coast combining with the super El Niño has amplified the sea level and also increased the chance of high flood. The distant waves were carried along with the wind movement crossing thousands of kilometers across the Pacific Ocean. Subsequently, when the swell approached the warmer ocean of Central America, it overlapped with the full moon high tide waves and created a massive surge throughout the region (https://ecoviva.org/large-swells-cause-damage-on-el-salvadors-coast/). The sea

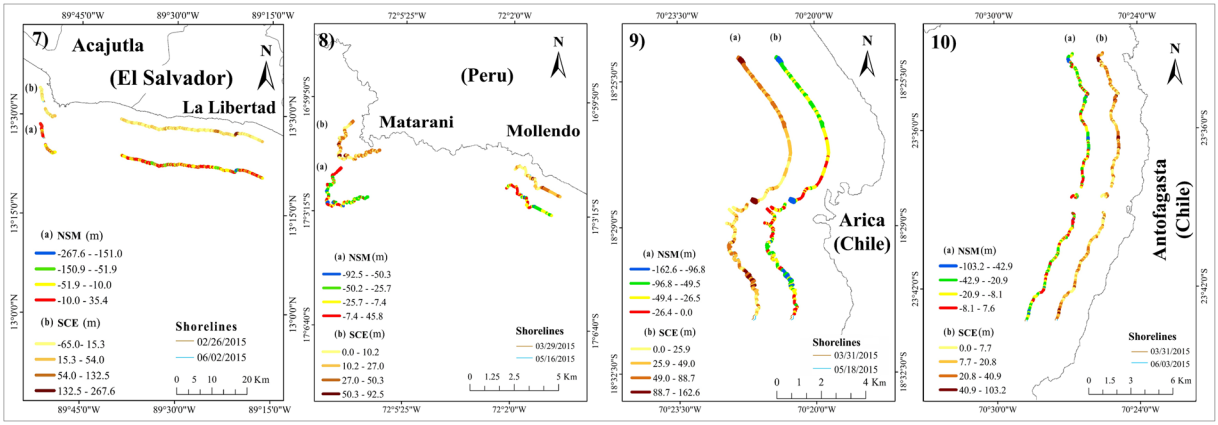

Fig. 4 (7–10) Shoreline change rates in the coastal regions of El Salvador, Peru, and Chile, showing (a) Net Shoreline Movement (NSM) and Shoreline Change Envelope (SCE)

level rise, ENSO phenomenon, along with the high tide waves has influenced the SSE to hit harder during the April–May 2015 and caused severe damages.

Documented damages to properties due to SSE

The wind generated by storms in the South Pacific had unloaded massive intense waves along the coasts of countries from Chile to Mexico. The devastating force of sea waves had inflicted chaos on coastal infrastructure, households, and small businesses. In Mazatlan (Mexico), the waves reached up to 3 mts, red flags were placed on the beaches, tourism were canceled, the hotel zone Dorada was flooded, waves reached up to Av. Camaron Sabalo, and the Torres Mazatlan hotel wall collapsed (https://www.debate.com.mx/mazatlan/Mar-de-fondo-causa-danos-en-Mazatlan-20150505-0059.html). In Lazaro Cardenas (Mexico), the waves reach up to 6 mts, one woman was reported dead, and few people were injured. All the beaches in the municipality were closed, and water entered the kitchen of all establishments in Playa Erendira in the region (http://www.cambiodemichoacan.com.mx/nota-252607). In the State of Guerrero (Mexico), 535 homes were damaged, which includes 2 from Acapulco beach, damages reported in 8 municipalities, 19 smaller vessels were damaged and 62 people were rescued in Acapulco, and one person was reported dead in Revocadero beach (http://cinabrio.over-blog.es/2015/05/danos-por-mar-de-fondo-continuan-castigando-costa-pacifica-de-mexico.html). In Huatulco (Mexico), the buoy system which serves as a signal to protect the reefs was destroyed with a huge economic loss, one dead body was found near Bahias de Huatulco beach, and 8 municipalities and 30 beaches were affected with tourist entities. Near Puerto Angel (Mexico), 30 restaurants were flooded, the water entered the streets, and all the beaches were closed temporarily in the region (https://www.gob.mx/conanp/prensa/mar-de-fondo-afecto-senalizacion-de-proteccion-de-arrecifes-en-bahias-de-huatulco). In Salina Cruz (Mexico), the Municipal Public Security reported that economic loss and material damages were recorded, a van was dragged towards the sea and a boat was overturned, and the restaurants and the beach areas were flooded with water and sand (http://expresionnoticias.blogspot.com/2015/05/continuara-mar-de-fondo-en-costas-de.html).

El Salvador was hit by waves that were above 2 mts and left dozens of victims, evacuees, and damage to infrastructure. Puerto de La Libertad coast was highly damaged due to waves, and the subsequent flooding caused 150 mts of inundation on Mizata beach. Tourism was suspended in El Salvador, 1367 persons were evacuated, 937 homes were damaged, 242 homes were destroyed, 66 homes were flooded, 60 restaurants were damaged, wells and crops were destroyed, and 1 person was reported missing (https://reliefweb.int/sites/reliefweb.int/files/resources/MDRSV008do1.pdf). In Peru, the waves reached up to 6 mts which deposited garbage along the coast of Lima, homes and roads were flooded in Callao, more than 82 minor ports were closed, a 60 mts long structure of nineteenth century was damaged in Pacasmayo port, 14 homes were destroyed, 80 was damaged near the Huanchaco town, 55 homes were damaged in Chimbote (near Matarani at Callao), 19 homes were damaged, and the port was flooded causing evacuation in the region

Table 2 Summary of coastline dynamics along the study area and its maximum wave heights recorded in the tide gauges

Location	No. of transects	NSM (%)			SCE (m)	Maximum inundation (m)	Maximum wave height (mts)			Remarks
		Landward movement	Stable	Seaward movement			Event 1	Event 2	Event 3	
Mexico										
Mazatlan (Mz)	377	33.2	3.7	63.1	0 to 62.2	53.9	1.69	1.64	0.73	Low risk of erosion
Lazaro Cardenas (Lc)	200	84.0	8.0	8.0	0 to 124.9	124.9	0.58	0.71	0.54	High risk of erosion
Acapulco (Ac)	1269	72.9	8.7	18.4	0 to 253.4	253.4	0.77	0.77	0.91	High risk of erosion
Puerto Angel (Pa)	148	57.4	35.8	6.6	0 to 46.6	46.6	1.60	1.21	1.36	Medium risk of erosion
Huatulco (Ht)	335	80.3	3.0	16.7	0 to 114.5	91.8	1.43	1.28	1.13	High risk of erosion
Salina Cruz (Sz)	212	44.3	22.6	33.1	0 to 33.0	33.0	1.64	1.33	1.27	Medium risk of erosion
El Salvador										
Acajutla	1102	74.5	11.7	13.8	0 to 267.6	267.6	2.25	2.12	2.35	High risk of erosion
Peru										
Matarani (Mt)	201	76.1	15.9	8.0	0 to 92.5	92.5	1.64	1.17	1.29	High risk of erosion
Chile										
Arica (Ar)	320	99.4	0.6	0	0 to 162.6	162.6	1.91	1.30	1.32	High risk of erosion
Antofagasta (Af)	414	84.1	12.3	3.6	0 to 103.2	103.2	1.33	1.17	1.36	High risk of erosion

(https://perureports.com/ocean-swells-damage-coastal-regions-from-north-to-south/884/). In Chile, the sea swell affected the northern and central part of the country from Arica to Puerto Montt, the waves reached a height of 3 to 4 mts, and the tourism was suspended subsequently. One person was reported dead near Cartagena coast who was swept away by the waves, and red alert was raised for the coastal cities (https://www.t13.cl/noticia/nacional/intensas-marejadas-afectan-borde-costero-del-pais).

Conclusion

The present study provides an optical view of coastal inundation along the coastal cities of Latin American countries before and after the SSE, which took place during April–May 2015 revealing the vulnerability of these low-lying coastal cities. Attempts has been made for the first time to measure the inundation limit and coastline changes due to a series of sea swell events using remote sensing techniques combined with the DSAS, an extension of ArcGIS tool. Moreover, this study focused mainly on Landsat_7 (ETM+) and Landsat_8 (OLI/TIRS) satellite data and MNDWI for the changes in shoreline regions. The NSM shows the maximum inundation limits (268 and 254 mts) for the coasts of El Salvador and Acapulco (Mexico) that were highly vulnerable followed by other cities. SCE variation indicated the maximum variation in coastline for different locations with the highest value of 268 mts for El Salvador. The results highlight the efficiency and importance of above mentioned methods in providing valuable evidence on coastal zone management. The study requires further detailed analysis using the Digital Elevation Models and SLR anomaly to increase the precision of composite shoreline dynamics.

Acknowledgments MPJ thank the Sistema Nacional de Investigadores (SNI), CONACyT, Mexico. PGP and FRH thank CONACyT for the research fellowship. Thanks to Dr. V.C. Shruti for her initial idea in this work. This article is the 110th contribution (partial) from the Earth System Science Group (ESSG), Chennai, India (participating members: PGP, JMP, GM, CL).

References

Álvarez-Gómez, J. A., Aniel-Quiroga, Í., Gutiérrez-Gutiérrez, O. Q., Larreynaga, J., González, M., Castro, M., Gavidia, F., Aguirre-Ayerbe, I., González-Riancho, P., & Carreño, E. (2013). Tsunami hazard assessment in El Salvador, Central America, from seismic sources through flooding numerical models. *Natural Hazards and Earth System Sciences, 13*(11), 2927–2939.

Becker, M., Karpytchev, M., & Papa, F. (2019). Hotspots of relative sea level rise in the tropics. *Tropical Extremes: Natural Variability and Trends, 7*, 203–262.

Brakenridge, G. R., Syvitski, J. P. M., Overeem, I., Higgins, S. A., Kettner, A. J., Stewart-Moore, J. A., & Westerhoff, R. (2013). Global mapping of storm surges and the assessment of coastal vulnerability. *Natural Hazards, 66*, 1295–1312.

de Farias, E. G. G., Lorenzzetti, J. A., & Chapron, B. (2012). Swell and wind-sea distributions over the mid-latitude and tropical North Atlantic for the period 2002–2008. *International Journal of Ocean, 306723*, 8.

Delgado-Serrano, M. del M., Mistry, J., Matzdorf, B., & Leclerc, G. (2017). Community-based management of environmental challenges in Latin America and the Caribbean. *Ecology and Society, 22*(1). https://doi.org/10.5751/ES-08924-220104.

Dereli, M. A., & Tercan, E. (2020). Assessment of shoreline changes using historical satellite images and geospatial analysis along the Lake Salda in Turkey. *Earth Science Informatics*. https://doi.org/10.1007/s12145-020-00460-x.

Foody, G. M. (2000). Estimation of sub-pixel land cover composition in the presence of untrained classes. *Computational Geosciences, 26*(4), 469–478.

Halabisky, M., Moskal, L. M., Gillespie, A., & Hannam, M. (2016). Reconstructing semi-arid wetland surface water dynamics through spectral mixture analysis of a time series of Landsat satellite images (1984–2011). *Remote Sensing of Environment, 177*, 171–183.

Hamlington, B. D., Cheon, S. H., Thompson, P. R., Merrifield, M. A., Nerem, R. S., Leben, R. R., & Kim, K.-Y. (2016). An ongoing shift in Pacific Ocean sea level. *Journal of Geophysical Research, Oceans, 121*, 5084–5097.

Himmelstoss EA, Henderson RE, Kratzmann MG, Farris AS (2018) *Digital Shoreline Analysis System (DSAS) version 5.0 user guide*: U.S. Geological Survey Open-File Report 2018–1179: 110 p.

Hoeke, R. K., McInnes, K., Kruger, J., McNaught, R., Hunter, J., & Smithers, S. G. (2013). Widespread inundation of Pacific Islands by distant-source wind-waves. *Global and Planetary Change, 108*, 1–11.

Hu, S., & Fedorov, A. V. (2016). Exceptionally strong easterly wind burst stalling El Niño of 2014. *Proceedings of the National Academy of Sciences, 113*(8), 2005–2010.

Jeihouni, M., Kakroodi, A. A., & Hamzeh, S. (2019). Monitoring shallow coastal environment using Landsat/altimetry data under rapid sea-level change. *Estuarine, Coastal and Shelf Science, 224*, 260–271.

Jiang, H., & Chen, G. (2013). A global view on the swell and wind sea climate by the Jason-1 Mission. A Revisit. *Journal of Atmospheric and Oceanic Technology, 30*, 1833–1841.

Kelly, J. T., & Gontz, A. M. (2018). Using GPS-surveyed intertidal zones to determine the validity of shorelines

automatically mapped by Landsat water indices. *International Journal of Applied Earth Observation and Geoinformation, 65*, 92–104.

Lyddon, C. E., Brown, J. M., Leonardi, N., & Plater, A. J. (2019). Increased coastal wave hazard generated by differential wind and wave direction in hyper-tidal estuaries. *Estuarine, Coastal and Shelf Science, 220*, 131–141.

Martin, J. A., Carreras, D., Pons, G. X., & Almaraz, A. (2020). Shoreline historical evolution (1956-2015) of beaches of enorca (Balearic Islands). In G. Malvarez & F. Navas (Eds.), *Global coastal issues of 2020*, *J Coast Res* (Vol. 95, pp. 563–567).

Muis, S., Verlaan, M., Winsemius, H. C., Aerts, J. C. J. H., & Ward, P. J. (2016). A global reanalysis of storm surge and extreme sea levels. *Nature Communications, 7*(11969), 1–11.

NOAA National Centers for Environmental Information, State of the Climate: Hurricanes and Tropical Storms for Annual 2015, published online January 2016, retrieved on May 16, 2019 from Https://Www.Ncdc.Noaa.Gov/Sotc/Tropical-Cyclones/201513.

Olthof, I., Fraser, R. H., & Schmitt, C. (2015). Landsat-based mapping of thermokarst lake dynamics on the Tuktoyaktuk Coastal Plain, Northwest Territories, Canada since 1985. *Remote Sensing of Environment, 168*, 194–204.

Páez-Osuna, F., Sanchez-Cabeza, J. A., Ruiz-Fernández, A. C., Alonso-Rodríguez, R., Piñón-Gimate, A., Cardoso-Mohedano, J. G., Flores-Verdugo, F. J., Carballo-Cenizo, J. L., Cisneros-Mata, M. A., & Álvarez-Borrego, S. (2016). Environmental status of the Gulf of California: a review of responses to climate change and climate variability. *Earth-Science Reviews, 162*, 253–268.

Palmer, K., Watson, C., & Fischer, A. (2019). Non-linear interactions between sea-level rise, tides, and geomorphic change in the Tamar Estuary, Australia. *Estuarine, Coastal and Shelf Science, 225*, 106247.

Reguero, B. G., Losada, I. J., Díaz-Simal, P., Méndez, F. J., & Beck, M. W. (2015). Effects of climate change on exposure to coastal flooding in Latin America and the Caribbean. *PLoS One, 10*, 1–19.

Rojas, O., Mardones, M., Rojas, C., Martínez, C., Flores, L., & Aguayo, M. (2017). Urban growth and flood disasters in the coastal river basin of South-Central Chile (1943-2011). *Sustainability, 9*(2), 195.

Scott, A. S., & Ramsay, D. L. (2014). Extreme cyclone wave climate in the Southwest Pacific Ocean: influence of the El Niño Southern Oscillation and projected climate change. *Global and Planetary Change, 123*(A), 13–26.

Sheik, M., & Chandrasekar. (2011). A shoreline change analysis along the coast between Kanyakumari and Tuticorin, India, using digital shoreline analysis system. *Geo-spatial Information Science, 14*(4), 282–293.

Sweet, W. V., Park, J., Gill, S., & Marra, J. (2015). New ways to measure waves and their effects at NOAA tide gauges: a Hawaiian -network perspective. *Geophysical Research Letters, 42*, 9355–9361.

Vitousek, S., Barnard, P. L., Fletcher, C. H., Frazer, N., Erikson, L., & Storlazzi, C. D. (2017). Doubling of coastal flooding frequency within decades due to sea-level rise. *Scientific Reports, 7*, 1–9.

Wang, X., Liu, Y., Ling, F., & Xu, S. (2018). Fine spatial resolution coastline extraction from Landsat-8 OLI imagery by integrating downscaling and pan sharpening approaches. *Remote Sensing Letters, 9*(4), 314–323.

Wdowinski, S., Bray, R., Kirtman, B., & Wu, Z. (2016). Increasing flooding hazard in coastal communities due to rising sea level: case study of Miami Beach, Florida. *Ocean and Coastal Management, 126*, 1–8.

Wong PP, Losada IJ, Gattuso JP, Hinkel J, Khattabi A, McInnes KL, Saito Y, Sallenger A, Cheong SM, Dow K, Duarte CM, Ebi KL, Faulkner L, Isobe M, Middel-burg J, Moser S, Pelling M, Penning-Rowsell E, Seitzinger S, Stive M, Tol RSJ, Vafeidis A (2014) Coastal systems and low-lying areas, climate change 2014: impacts, adaptation and vulnerability. In Field CB, Barros VR, Dokken DJ, Mach KJ, Mastrandrea MD, Bilir TB, Chatterjee M, Ebi KL, Estrada YO, Gen-ova RC, Girma B, Kissel ES, Levy AN, MacCracken S, Mastrandrea PR, White LL (eds). *Global and sectoral aspects: working group contribution to the fifth assessment report of the inter-governmental panel on climate change*. Cambridge, UK and New York, USA. 361–409.

Xavier, C.-C., Cecilia, E., Vanesa, P., Ismael, M.-T., & Cristóbal, R.-H. (2019). Pacific coast of Mexico. *World Seas: an Environmental Evaluation, 28*, 655–671.

Yu, L., Wu, X., Zheng, X., Zheng, T., Xin, J., & Walther, M. (2019). An index system constructed for ecological stress assessment of the coastal zone: a case study of Shandong, China. *Journal of Environmental Management, 232*, 499–504.

Zuniga, E., & Magaña, V. (2018). Vulnerability and risk to intense rainfall in Mexico: the effect of land use cover change. *Investment Geo, 95*.